

0278-4343(94)E0030-P

Distributions of the sea-surface temperature fronts in the Baltic Sea as derived from satellite imagery

MATI KAHRU, *† BERTIL HÅKANSSON‡ and OVE RUD*

(Received 25 November 1992; in revised form 22 December 1993; accepted 8 March 1994)

Abstract—A 9-month time series of satellite infrared imagery was used to examine the sea surface temperature (SST) variability in the northern and central Baltic Sea. Objective multi-level edge detection techniques were applied to find sharp SST gradient areas known as fronts. The spatial distribution of frontal frequency was calculated over time periods from a few days to 9 months covering different thermal and wind conditions. The 9-month average frequency that a front is detected in a pixel of 1.1 × 1.1 km is up to 10% in certain areas whereas the median is around 2%. Large scale fronts are aligned to the coast and isobaths, and occur predominantly in areas of straight and uniformly sloping bottom topography. The major frontal areas are along the eastern coast of the Bothnian Sea and along the north-western coast of the Gulf of Finland. Low large-scale frontal frequency is characteristic to areas with highly structured bottom topography. The major mechanism of front generation is coastal upwelling, being complemented by coastal jets, eddies, differential heating and cooling, and water exchange between basins with different water characteristics. Filaments ("squirts") originating from upwelling areas are shown to be an important mechanism for transporting water and substances over long distances.

INTRODUCTION

SATELLITE images of the sea surface temperature (SST) field obtained from the Advanced Very High Resolution Radiometer (AVHRR) on polar-orbiting NOAA satellites provide information on the meso-scale thermal structures unparalled by traditional shipborne observations (ABBOTT and CHELTON, 1991). However, due to various reasons the systematic use of analysis of the satellite SST data has been hindered in the past (CORNILLON *et al.*, 1987). In recent years efforts have been made to use image processing techniques such as edge detection and automated feature extraction to aid in the analysis of the SST imagery (HOLYER and PECKINPAUGH, 1989; SIMPSON, 1990; CAYULA and CORNILLON, 1992).

Edge detection is one of the basic components of automated image analysis techniques. Different edge detectors have been developed (see Holyer and Peckinpaugh, 1989), mostly as discrete approximations to the gradient. Gradient-based edge detectors are characterized by spurious responses when applied to noisy data. These so-called local operators use one or another fixed threshold to distinguish an edge from "normal" variability. The multi-level (picture, window, local) approach offers more potential to adapt to different conditions and to detect atmospheric interference. As an example, the

^{*}Stockholm University, Department of Physical Geography, S-106 91 Stockholm, Sweden.

[†]Current address: Scripps Institution of Oceanography, UCSD, La Jolla, CA 92093-0218, U.S.A.

^{\$}Swedish Meteorological and Hydrological Institute, S-601 76 Norrköping, Sweden.

Cayula algorithm (Cayula, 1988; Cayula and Cornillon, 1992) uses the bimodality of the histogram in a local window as the basic edge detector. The resulting edge detection is based not on the absolute strength of the front gradient but on the separability of pixel values to different compact areas. In this paper the Cayula edge detection and cloud screening algorithm is used on a time series of the Baltic Sea SST images.

The Baltic Sea is a shallow, non-tidal, brackish estuary where the water masses are formed as a result of a cascade of mixing processes. In these conditions areas of strong gradients, known as fronts (Bowman and Iverson, 1978), are a common feature. In contrast to the well-known tidal fronts (Simpson and Hunter, 1974) the fronts in the Baltic cannot be predicted using simple criteria. The Baltic fronts have been occasionally observed using shipborne measurements (Elken et al., 1987; Pavelson, 1988) but due to their short-lived nature no basin-wide and/or seasonal coverage is available. Fronts are important as potential sites of intense vertical exchange of water and substances, locations of intensified biological and geochemical processes. Fronts in the Baltic Sea are known to be associated with increased primary productivity and elevated zooplankton abundance (Kahru et al., 1984, 1986). Satellite infrared and visible imagery (e.g. Horstmann, 1983) has great potential for the study of fronts; however, so far only a few studies (Gidhagen, 1987; Bychkova and Viktorov, 1984) have attempted quantitative analysis of the Baltic Sea imagery.

MATERIALS AND METHODS

AVHRR imagery

Figure 1 shows the study area with the geographical points of reference. AVHRR data analyzed in this study were captured at the Swedish Meteorological and Hydrological Institute (Norrköping, Sweden). Most of the images were archived during the Swedish-Finnish multi-disciplinary Gulf of the Bothnia Year 1991. Images of 1024×1024 pixels were corrected for geometric distortion and registered to the Mercator projection with a spatial resolution of 1.1 km. The geo-location of the image was checked by overlaying a "standard" coastline image. If necessary, the image was shifted relative to the contour overlay achieving ± 2 pixel accuracy between subsequent images. Data from AVHRR channels 1, 4 and 5 were recorded. A total of 108 sufficiently cloud-free scenes between 24 June 1991 and 3 March 1992 were used.

The radiation temperature from AVHRR channel 4 (11.5–12.5 μ m) was used as an estimate of the SST. The radiometric resolution of the data was 0.125°C. While multichannel techniques (McClain *et al.*, 1985) are known to give better absolute temperature values, they also introduce a considerable amount of noise and distort the SST gradient magnitude (La Violette and Holyer, 1988).

Atmospheric disturbances are known to be the major source of error in the SST estimates. Thin clouds, sub-pixel clouds, haze and fog produce features that can mistakenly be taken as fronts, and must be separated from the real SST fronts.

Edge detection/cloud screening

The front detection process used here is an implementation of the algorithm developed by CAYULA (1988) and CAYULA and CORNILLON (1992) with simple modifications. The algorithm consists of several modules and deals with both cloud and edge detection. Only a concise description is given below, more can be found in the references listed above.

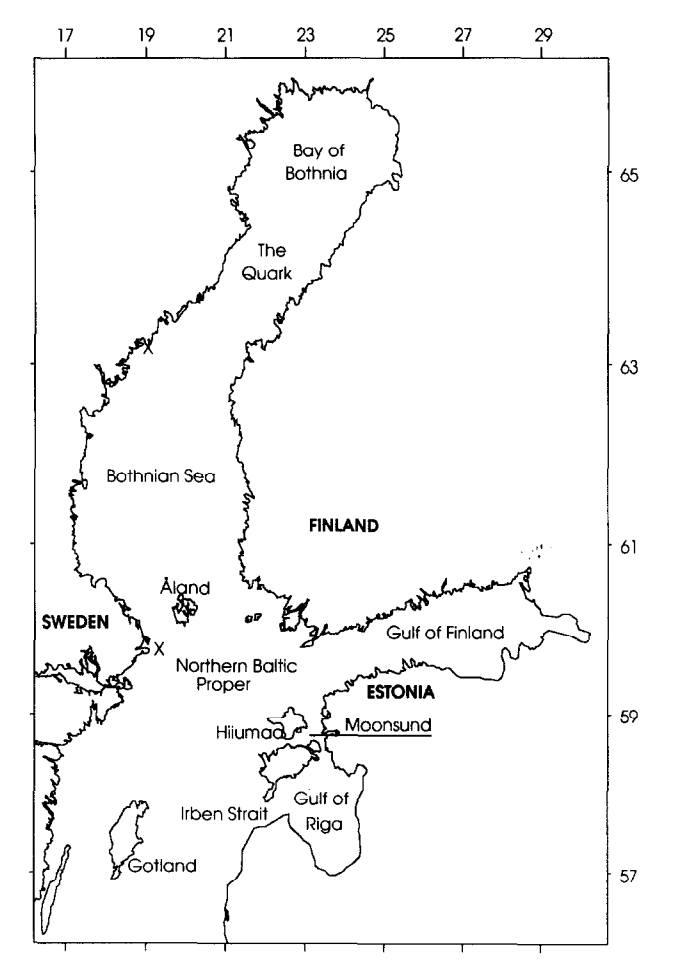


Fig. 1. The study area with the locations of wind measurements (X).

The cloud detection and elimination modules work in series and use several properties of clouds that differentiate them from the underlying sea surface. If a pixel or a pixel area does not pass a test, it is marked as invalid and not used in the subsequent analysis.

Under conditions of strong solar irradiance and low windspeed, strong vertical gradient is formed in the thin top layer (Schluessel et al., 1988) causing the appearance of "hot spots" which reflect the local boundary layer meteorology rather than the water masses beneath them. The original Cayula algorithm often detected "hot spot" edges as SST fronts. To prevent that, a valid threshold range for the SST values was determined visually for each image, and the values outside the range were masked.

The next test uses the fact that areas of small clouds have high gradients with variable direction whereas sea surface areas have coherent gradient directions which form elongated shapes. The image was median-filtered with a 3×3 window and roughly segmented into separate connected regions (segments) depending on the gradient magnitude. Segments with coherent gradient vectors and/or with elongated shape (larger eigenvalue of the spatial covariance matrix divided by the smaller eigenvalue) were

classified as sea whereas areas with low gradient coherence and "bulky" shape were classified as clouds.

Histograms from valid pixel values in overlapping windows of 32 ×32 pixels were computed and studied for bimodality. The best threshold value separating the two potential populations was found. Bimodality of the histogram was accepted only if the difference between the two medians was more than 3 digital units. If bimodality was confirmed, the spatial cohesion of the two populations was tested. The window was marked as containing an edge if the two populations formed compact areas, otherwise the bimodality was considered due to noise. An edge image was constructed for the confirmed edge windows from pixels which contacted both populations. Finally, small gaps between edge pixels were attempted to fill up by following the gradient image and isolated edges less than 15 pixels in size were eliminated.

Frontal frequencies

As clouds practically always cover a significant part of the study area, some kind of compositing was needed to get a representative front distribution over the whole area. This was done by accumulating consecutive front images and the corresponding cloud free areas until the whole area was covered. It was assumed that the frontal patterns did not change significantly during the period of compositing. Then the front frequency was found as the ratio of the sum of accumulated front pixels to the sum of accumulated cloud free pixels over the windows of 4×4 pixels. The spatial averaging involved here should also correct for the positioning error of 1–2 pixels between subsequent images. The resulting images are consequently reduced in size to 256×256 pixels.

EOF analysis

Complex spatio-temporal distributions can be decomposed into orthogonal components using empirical orthogonal function (EOF) analysis (Kelly, 1988). The singular value decomposition method of Kelly (1985) was used to compute EOFs from the series of frontal frequency images. The EOFs can be ranked by their temporal, spatial or total variance. In this application we were looking for reoccurring frontal patterns (spatial modes) ranked either by variance. The temporal development of the amplitude of these patterns can give some clue to find the dominant relationships between the forcing functions and the front patterns.

Winds

Wind data recorded at two coastal weather stations (Fig. 1) were obtained from the Swedish Meteorological and Hydrological Institute.

RESULTS

Frontal frequencies

An example of the results of the front detection program on a subarea of an SST image is shown on Fig. 2. The major source of temperature gradients in the summertime Baltic Sea

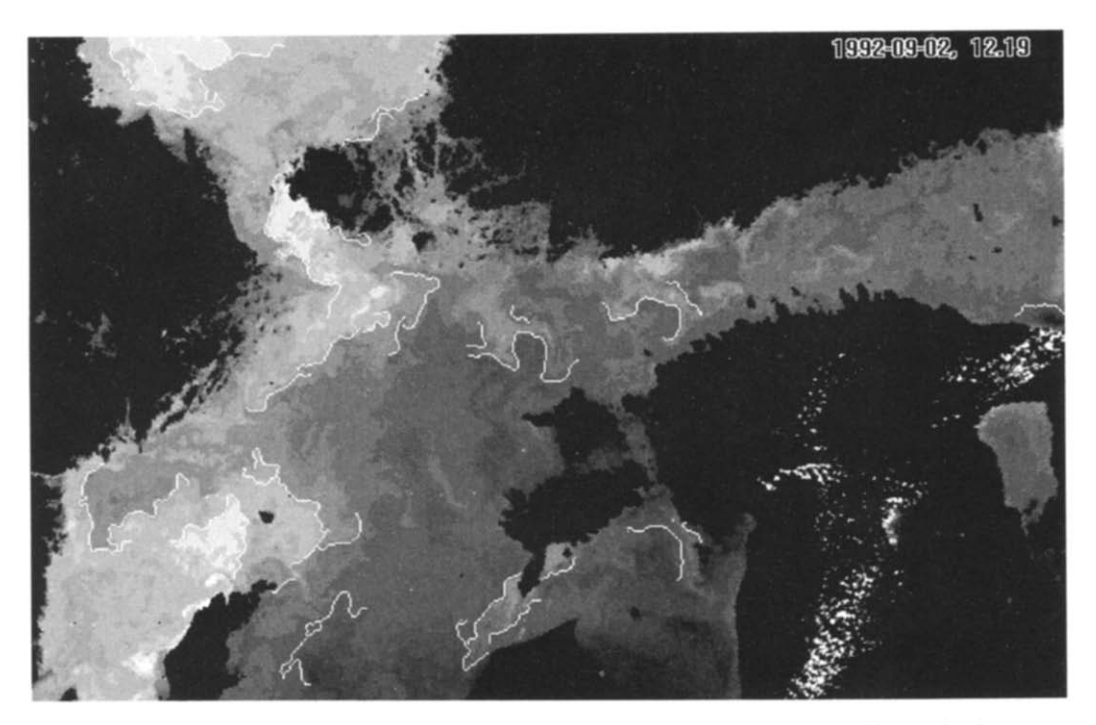


Fig. 2. Results of the front detection program on an AVHRR channel 4 subimage in the Northern Baltic Proper and western Gulf of Finland on 2 September 1992 (UTC 12.19). Brighter shades of gray correspond to colder, and darker shades to warmer, water. The detected fronts are overlaid as white contours. Land is considerably warmer and looks black. A few small scattered clouds are seen over land.

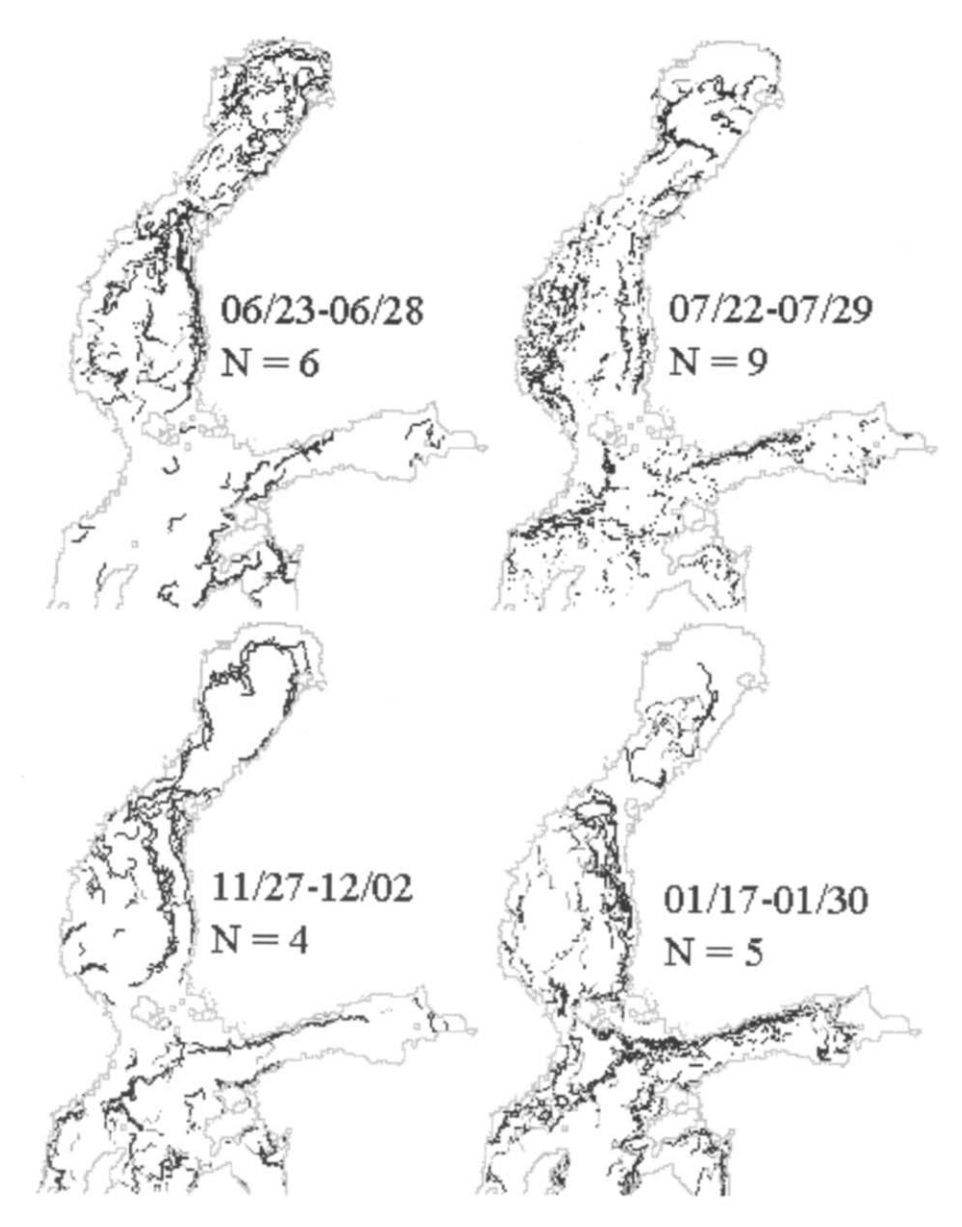


Fig. 3. Examples of composited frontal frequency distributions. Pixels with higher than 4% frontal frequency are shown. The time period (Month/Day–Month/Day) and the number of images (N) used for compositing are shown.

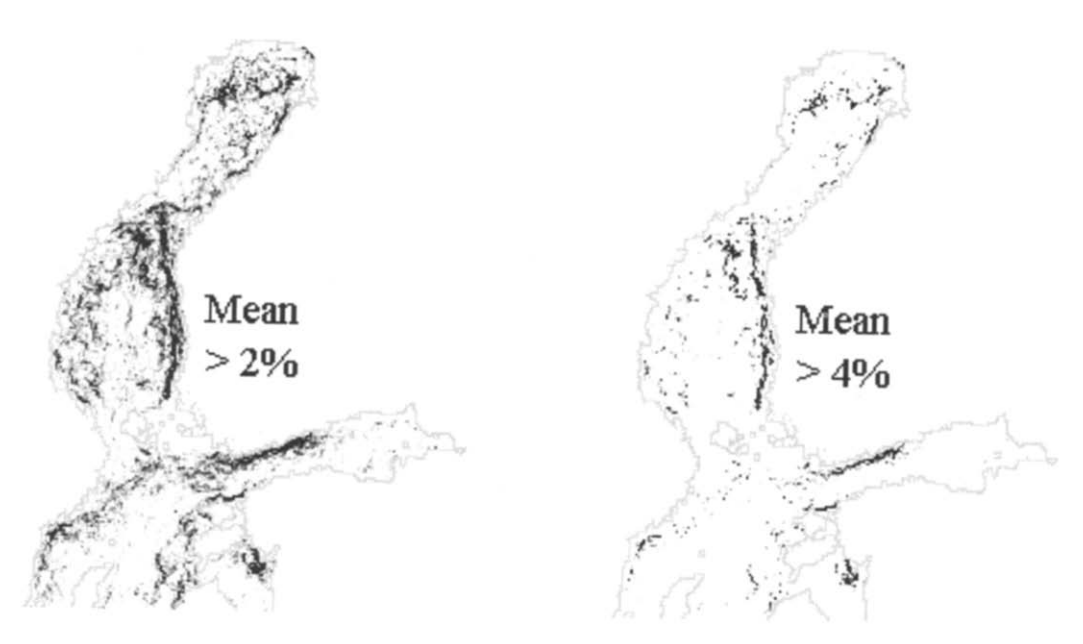
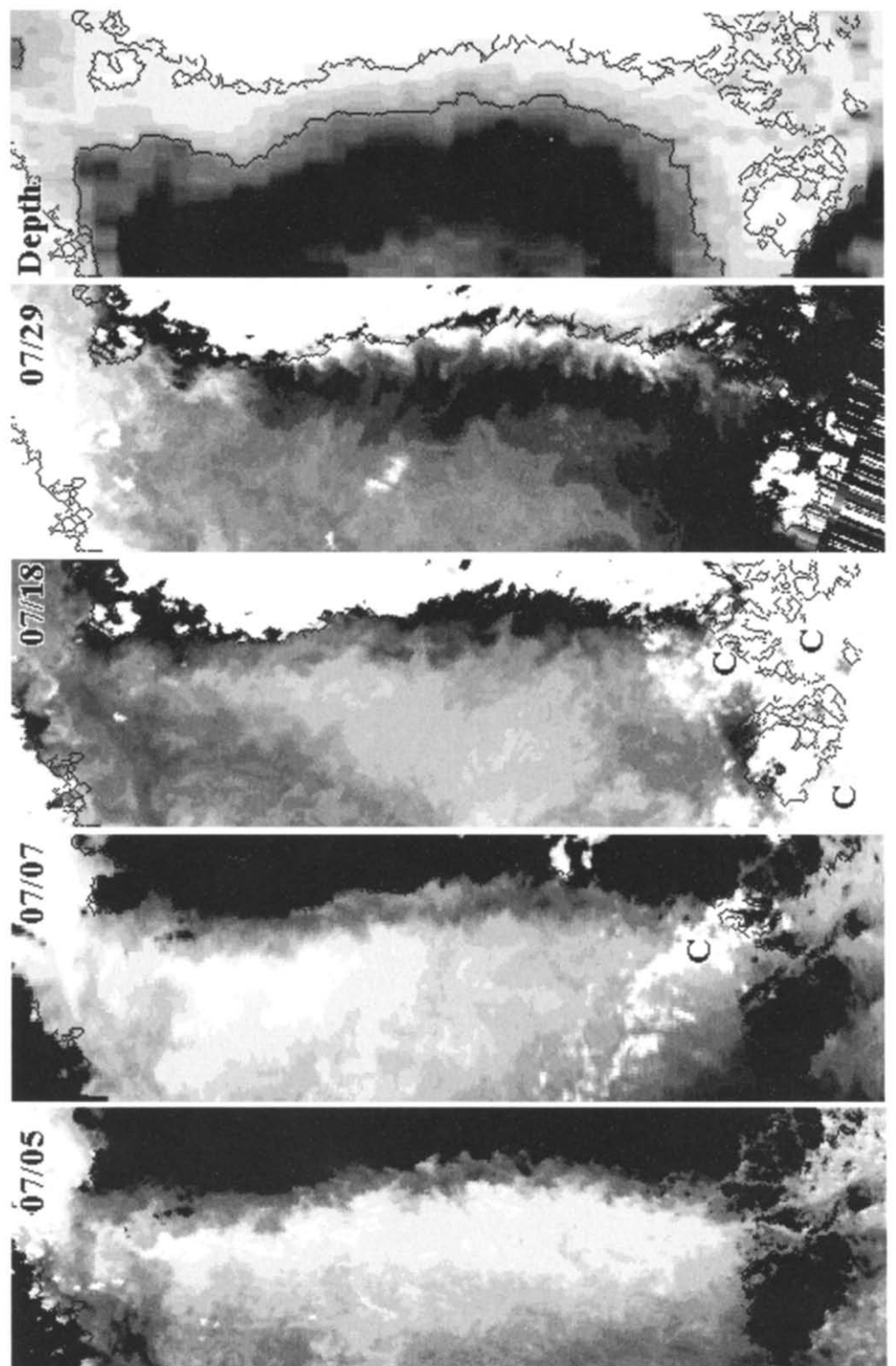


Fig. 4. Average frontal frequency distribution between 23 June 1992 and 2 March 1992. Left panel: frequency above 2% shown; right panel: frequency above 4% shown.



Sea-surface temperature dynamics along the eastern coast of the Bothnian Sea in July 1991: (from left to right) 5 July 16.24, 7 July 05.45, 18 July 02.51, 29 July 02.25 (dropout lines near the bottom), depth (50-m depth contour shown, areas deeper than 100 m black). C—clouds. Fig. 6.

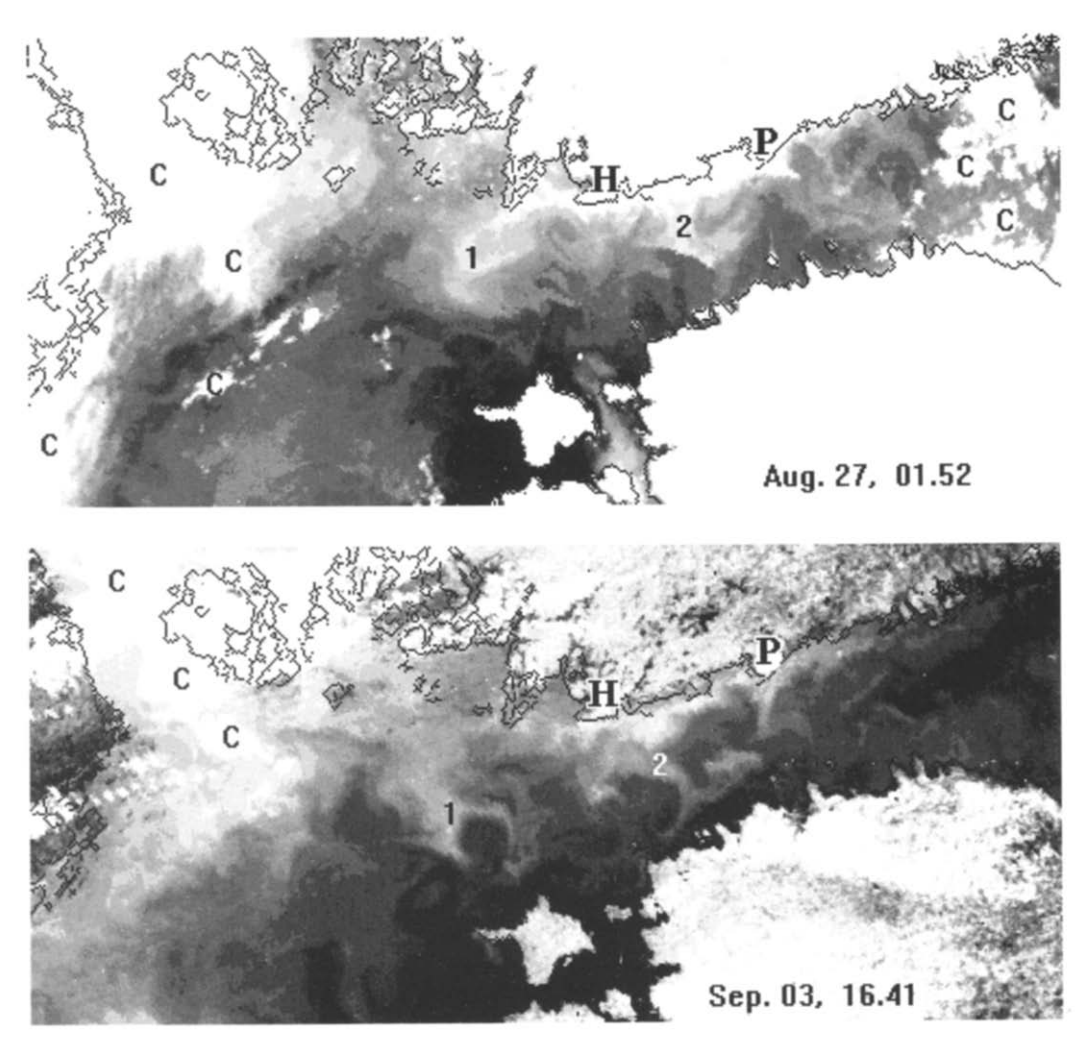


Fig. 7. Sea-surface temperature patterns showing the formation of upwelling filaments along the northwestern coast of the Gulf of Finland. The filaments marked as 1 and 2 have emerged from the upwelling centers, respectively, off Hangö (H) and Porkkala (P). C—clouds.

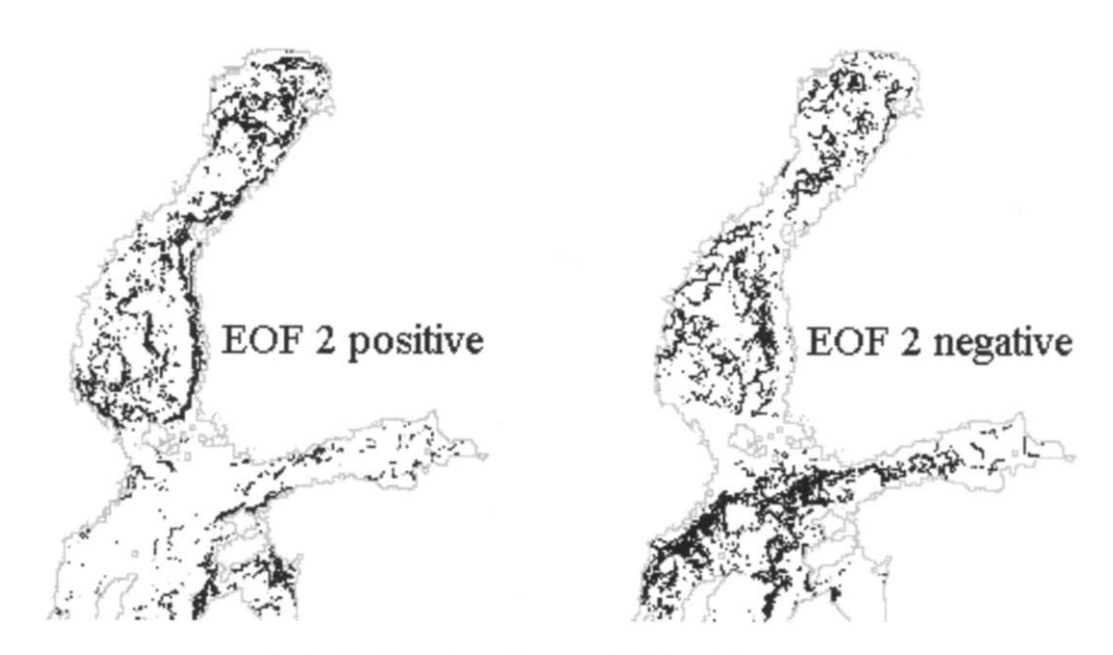


Fig. 9. Positive and negative parts of EOF mode 2.

images	
Period (month/date)	No. of images composited
06/23-06/28	6
07/03-07/04	4
07/05-07/05	4
07/06-07/08	8
07/1407/18	7
07/22-07/29	9
07/30-08/06	15
08/13-08/14	6
08/22-09/03	12
09/16-09/28	7
10/03-10/08	4
10/13-10/26	6
11/10-11/17	7
11/27-12/02	4
01/17-01/30	5
02/17-03/02	4

Table 1. Composited frontal frequency images

imagery is known to be upwelling (Gidhagen, 1987). Large areas with cold upwelled water can be seen southwest of Åland and north of Gotland. Smaller upwelling plumes are visible along the northwestern coast of the Gulf of Finland and in the Irben strait. Most of the fronts that have been detected are evidently caused by recent upwelling events. The algorithm has performed satisfactorily and selected most of the "front-like" features while discarding other gradient areas.

By compositing over 4–15 adjacent individual front images altogether 16 frontal frequency images were obtained (Table 1). Some examples are shown on Fig. 3. An average over all the composited frontal frequency images displays the average frontal frequency over the 9-month study period in the northern and central Baltic Sea (Fig. 4). It is apparent that fronts occur much more frequently in certain areas compared to other areas. Histogram of the average frontal frequency (Fig. 5) shows that, as a 9-month average, the probability that a front is detected in a particular pixel area of 1.1×1.1 km is up to 10% for the most frequent front regions whereas the median frequency is around 2%. On individual image composites the frequencies are naturally higher. As the frontal frequency is calculated over windows of 4×4 pixels, the maximum frequency is 25% in case of a single straight front across the window. On Fig. 3 the frequencies above 4% are shown.

It is obvious from Fig. 4 that the large-scale distribution of frontal frequency is aligned to the coast and follows the local bottom topography. It is equally evident that some coasts have higher frequency of fronts than others. The major large-scale frontal areas are along the eastern coast of the Bothnian Sea extending northwards into the Quark Strait, in the Gulf of Finland along its northwestern coast extending southwest to the coast of Sweden, off the Western Estonian archipelago extending south along the Baltic east coast. Low frontal frequency is characteristic of the southern and eastern Gulf of Finland, western Gulf of Riga, central parts of the Northern Baltic Proper and the Bothnian Sea, southwestern part of the Bay of Bothnia.

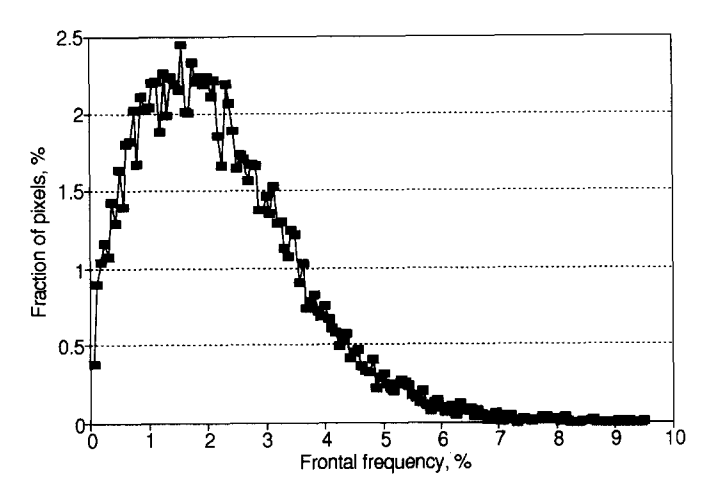


Fig. 5. Histogram of the average frontal frequency. Frontal frequency is defined as the frequency that a pixel of 1.1×1.1 km is detected as a front pixel.

The north-south fronts along the eastern coast of the Bothnian Sea, often forming parallel bands along the coast, were persistent under various wind directions and seasons, and are collectively referred to as the Eastern Bothnian Sea Front. The distance between the bands increased northwards where the offshore band bended more westward following the 100-m isobath. In contrast to the east coast, the fronts in the western Bothnian Sea were small, scattered, and did not form definite bands along the coast. This is consistent with the highly structured and irregular bottom slope in the western part of the Bothnian Sea.

Another major front area in the northwestern Gulf of Finland was caused by frequent upwellings and the associated fronts. The major frontal regions were aligned to the relatively straight and uniformly sloping bottom topography. During the cooling season starting in September, the area of frequent fronts was often extended southwest across the Northern Baltic Proper, connecting with the fronts along the coast of Sweden (Fig. 3). These fronts across the northern Baltic Proper roughly followed the 50-m isobath.

The fronts off the Western Estonian archipelago were smaller in spatial extent and more variable in time; however, the frequent fronts were again tied to relatively straight areas of the coastal slope (e.g. northeast of Hiiumaa).

Highly frequent but small-scale fronts were often found in the vicinity of straits connecting basins with outflows of low-salinity water (Irben strait, Moonsund) or river mouths (in the Gulf of Riga).

Examples of frontal dynamics

In late June and early July many of the fronts followed isobaths between shallow and deeper areas, and were apparently caused by increased heating of the surface layer in the shallow areas.

In the Bothnian Sea, warmer waters in the shallow areas around the basin surrounded

the cooler central waters. The warm water band along the eastern coast of the Bothnian Sea was narrower (10-20 km) and more uniform than the similar warm waters along the west coast, which is consistent with the more regular bottom topography along the east coast. The temperature gradient was especially enhanced by the coolest water spread along the seaward flank of the warm band (Fig. 6, 5-7 July). When the weak (2-7 m s⁻¹) south-westerly winds turned into northerly winds (5-9 m s⁻¹) around 4 July and became upwelling-favourable, a narrow stripe of cool water emerged between the warm band and the coast. At the same time the cool water plume offshore the warm band expanded considerably (Fig. 6, 7 July). Frontal upwelling at the seaward flank of the warm band was a probable source of cool water. The warm water band became separated by fronts from both sides. Upwelling disappeared by July 14 when the winds had turned southwest again. The front along the seaward side of the warm water band had become unstable and disintegrated into a sequence of interleaved warm and cool water blobs (Fig. 6, 18 July). By the end of July upwelling centers had reappeared along the coast and the structure of a warm band separated by colder waters and the associated fronts on its both sides was reestablished (cf. 29 July on Fig. 6 and 22–29 July on Fig. 3). Westward drift of the surface waters caused the warm band to increase in width to more than 60 km with the cold filaments of upwelled water plunging into it from the coast.

From a series of 10 images between 22 August and 3 September, the dynamics of the upwelling along the north-western coast of the Gulf of Finland can be followed in more detail. Two examples are shown on Fig. 7. Intense upwelling occurred along the coast and especially off the capes extending into the sea. The two most significant upwelling centers were located off Hangö and Porkkala. The cool upwelled water that was uplifted along the coast first drifted westward until being drawn into the eddy field. Filaments transported to the cold upwelled water southeast across the Gulf. While approaching the Estonian coast, the eastern filament (2 on Fig. 7) formed a counter rotating vortex pair, one of which turned west again. At the same time new filaments were emerging at the upwelling centers. Tracing the upwelling features allowed to detect that in about 10 days the waters upwelled along the northern coast had crossed the Gulf and were spreading along the southern coast.

EOF analysis

It was hoped that the time series of frontal frequencies could be decomposed into simple patterns interpretable in terms of the forcing functions. The EOF modes of the non-negative frontal frequency may have both positive and negative areas. A positive mode area corresponding to a positive amplitude corresponds to increased frontal frequency. Similarly, a negative mode area corresponding to a negative amplitude results in an increased frequency.

When decomposing the total spatio-temporal variance, the first EOF mode is practically identical to the mean frontal frequency pattern (Fig. 4) and contains 28.7% of the total variance. The amplitude of the EOF mode 1 (Fig. 8) shows how well the particular front pattern corresponds to the mean frontal frequency. The lowest amplitudes of mode 1 in August and end of July correspond to a period of weak and variable winds, "hot spots" and atmospheric haze.

The second EOF mode (Fig. 9) adds 8.2% of the total variance. Its positive part corresponds to, among others, the inshore band of the Eastern Bothnian Sea Front while

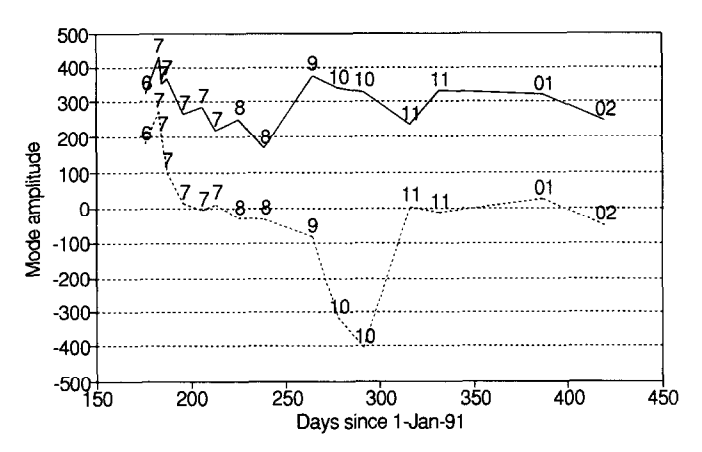


Fig. 8. Amplitudes of frontal frequency EOF modes 1 (solid line) and 2 (dotted line). The month number of the sample period is indicated on the line.

the negative part corresponds to the offshore band of the same front. The negative mode also represents fronts along the coast of Sweden and in the Northern Baltic Proper. As seen from the mode amplitude time series (Fig. 8), the positive part of mode 2 described the front patterns that occurred in June and early July, whereas the negative part of mode 2 was dominant in October. Mode 3 (not shown) added 7.1% of the total variance and described small-scale fronts all over the area (positive part) and some other less frequent fronts (negative part). When combined, modes 1–4 made up slightly over 50% of the cumulative variance. The results prove that the frontal distributions are spatially complicated and not easily reducible to combinations of a small number of components.

DISCUSSION

Reliability of automated front detection

Retrieval of the SST variability from infrared imagery is critically dependent upon the identification and removal of clouds and other atmospheric disturbances. Compact, thick clouds are usually easily removed whereas thin clouds, sub-pixel clouds and haze may cause significant errors. Automated cloud screening algorithms using the AVHRR near-infrared channel have been developed for daytime imagery (e.g. SIMPSON and HUMPHREY, 1990) but could not be used here due to the lack of channel 2 in recorded data.

The effect of increased atmospheric attenuation is known to lower the apparent SST and reduce the magnitude of SST gradients (Holyer and Peckinpaugh, 1989). The Cayula algorithm proved to be efficient in screening out small clouds and various noise in the data. However, edges caused by the distribution of haze and "hot spots" were often picked up as SST fronts by the algorithm. The distribution of "hot spots" show little resemblance to the "normal" SST spatial patterns, and primarily reflect local atmospheric conditions. Visual thresholding of the image had to be used to invalidate the "hot spot" areas. A simple automated procedure for "hot spot" removal using the difference between day and night images would be less useful in practice due to cloud interference. Although atmospheric

disturbances reduced the amount of pixels available and probably obscured some fronts in areas considered valid, it is believed that due to the many screening operations the percentage of "false" fronts is not significant. However, some interference in the late July and August imagery was inevitable. Small errors in the estimation of frontal frequency were caused even when an area was correctly marked as invalid but a front could not be detected due to its closeness to the cloud or land boundary (the front detection algorithm expects sufficient cloud-free areas on both sides of the potential front).

Observations using satellite infrared imagery are inevitably biased towards clear sky weather situations. It is difficult to estimate whether a hypothetical "all-weather" average frontal frequency would differ from the average based on the cloud-free images.

It must be noted that the definition of a front used here as the border zone between two compact areas of different temperature is not exactly equal to the conventional notion of oceanographers who also assume that the temperature step must be higher than a certain threshold level. However, temperature is only an indicator of the dynamically important density. In the Baltic Sea the salinity effect on density is usually dominant over the effect of temperature. Although a density front is almost always associated with a change in temperature as well (Pavelson, 1988), the temperature step across the density front can be arbitrarily small, thus invalidating a universally applicable threshold limit.

Implications of the results

Automatic detection of SST fronts represents an objective and efficient way to simplify the rich structure inherent in the SST field. The locations of high gradient areas reveal the results of different dynamical processes: coastal upwelling, differential heat loss or heat gain, currents, mixing of different water masses. Although fronts in the Baltic Sea have been studied from ships, it is only in the potential of satellite imagery to provide fully basinwide and seasonal coverage. The distributions of fronts as described here could be used to direct future *in situ* hydrographic studies because satellite observations alone are seldom capable of explaining phenomena. Eastern Bothnian Sea and northwestern Gulf of Finland are two such hydrographically active areas where intense vertical exchange of water and substances takes place and where detailed *in situ* studies are needed to explain the complex SST dynamics.

Areas of frequent large-scale fronts were invariably aligned to isobaths, being associated with relatively straight and uniform bottom slope. In contrast, indented coastline with highly structured bottom topography was associated with low frontal frequency.

In the eastern Bothnian Sea, although the character of the water masses, the exact locations of fronts as well as the probably physical mechanisms causing the fronts changed over time, the fronts persisted over widely varying wind and thermal conditions. The hydrodynamics of these fronts needs further studies. In a toxicity study of phytoplankton blooms over the Baltic, Kononen *et al.* (in press) found that the heavy blooms of cyanobacteria *Nodularia spumigena* that they observed along the eastern Bothnian Sea in August 1990 had the highest concentration of the toxin nodularin. It is probable that the Eastern Bothnian Sea Front is one of the key factors causing the emergence of the cyanobacterial blooms. It has been previously observed that fronts are associated with increased cyanobacterial productivity (Kahru *et al.*, 1984) and play a crucial role in cyanobacterial bloom formation (Kononen and Nõmmann, 1992).

The upwelling fronts in the northwestern Gulf of Finland were also present over

different weather conditions. The upwelling filaments that emerge when the upwelling front along the coast becomes unstable, are a common feature there. Upwelling filaments in the California Current are known to be important in the coastal-offshore transport (Flament et al., 1985). It can be concluded from a series of images analyzed in this work that the upwelling filaments in the Gulf of Finland are effective carriers of water and substances across the Gulf. It is probable that the transport due to the energetic filaments is much more important compared to the transport due to the sluggish mean circulation. However, as the time and space scales of the filaments are below the resolution of conventional hydrographic data, the mean circulation has been usually considered when discussing the transport of pollutants and other substances. The data available in this study imply that the filaments in the Gulf of Finland predominantly originate from the coast of Finland and move south towards the coast of Estonia, and not vice versa. The role of upwelling filaments in regard to transport of pollutants such as nuclear wastes, oil slicks and other hazardous substances definitely deserves more attention.

Although the biological implications of fronts such as increased primary productivity and increased zooplankton concentration have been observed, no quantitative estimates of the influence of fronts on the carbon cycling and nutrient balance are available. As argued by Woods (1988), the statistics of mesoscale events are needed to be included in models of primary production which are necessary for improving our understanding of carbon dioxide dynamics and climate change. Data from the forthcoming SeaWiFS ocean color mission measuring phytoplankton pigments (Hooker and Esaias, 1993) in combination with the SST fields from the NOAA/AVHRR scanner will hopefully provide a breakthrough in this topic.

Acknowledgements—The authors are indebted to Dr J.-F. Cayula for a listing of his edge detection program and to Drs William Emery and Terry Beaver for a listing of their EOF program. Most of the image analysis was done using WIM, an image analysis program developed by one of the authors (M. Kahru) for the Microsoft Windows environment. This project has partly been supported by the Swedish Environmental Protection Agency and the Swedish Institute.

REFERENCES

- ABBOTT M. R. and D. B. CHELTON (1991) Advances in passive remote sensing of the occan. *Review in Geophysics*, **29** (suppl), 571–589.
- BOWMAN M. J. and R. L. IVERSON (1978) Estuarine and plume fronts. In: Oceanic fronts in coastal processes, M. J. BOWMAN and W. E. ESAIAS, editors, Springer-Verlag, New York, pp. 87–104.
- BYCHKOVA I. A. and S. V. VIKTOROV (1987) Use of satellite data for identification and classification of upwelling in the Baltic Sea. *Oceanology*, 27, 158–162.
- CAYULA J.-F. (1988) Edge detection for SST images, M.S. Thesis, Department of Electrical Engineering, University of Rhode Island, 91 pp.
- CAYULA J.-F. and P. CORNILLON (1992) Edge detection algorithm for SST images. *Journal of Atmospheric and Oceanic Technology*, **9**, 67–80.
- CORNILLON P., C. GILMAN, L. STRAMMA, O. BROWN, R. Evans and J. Brown (1987) Processing and analysis of large volumes of satellite-derived thermal infrared data. *Journal of Geophysical Research*, **92**, 12,993–13.002.
- ELKEN J., L. TALPSEPP and J. PAVELSON (1987) Dynamics and distribution of water masses in the southern Gotland basin (polygon studies), 15th Conference of the Baltic Oceanographers, Copenhagen, 1, 251-263.
- FLAMENT P., L. ARMI and L. WASHBURN (1985) The evolving structure of an upwelling filament. *Journal of Physical Oceanography*, 90, 11,765-11,778.
- GIDHAGEN L. (1987) Coastal upwelling in the Baltic—satellite and in situ measurements of sea surface temperatures indicating coastal upwelling. Estuarine and Coastal Shelf Science, 24, 449–462.

- HOLYER R. J. and S. H. PECKINPAUGH (1989) Edge detection applied to satellite imagery of the oceans. *IEEE Transactions on Geoscience and Remote Sensing*, 27, 46–56.
- HOOKER S. B. and W. E. ESAIAS (1993) An overview of the SeaWiFS Project. EOS, 74, 241-246.
- HORSTMANN U. (1983) Distribution patterns of temperature and water colour in the Baltic Sea as recorded in satellite images: indicators of plankton growth. Berichte Institut für Meereskunde Universität Kiel, 106, 1–147
- KAHRU M., J. ELKEN, I. KOTTA, M. SIMM and K. VILBASTE (1984) Plankton distributions and processes across a front in the open Baltic Sea. *Marine Ecology Progress Series*, 20, 101–111.
- KAHRU M., S. Nōmmann, M. SIMM and K. VILBASTE (1986) Plankton distributions and processes in the Baltic boundary zones, In: *Marine interfaces ecohydrodynamics*, J. C. J. NIHOUL, editor, Elsevier, Amsterdam, pp. 273–294.
- Kelly K. A. (1985) The influence of winds and topography on the sea surface temperature distribution patterns over the northern California slope. *Journal of Geophysical Research*, **90**, 11,783–11,798.
- Kelly K. A. (1988) Comments on "Empirical orthogonal function analysis of advanced very high resolution radiometer surface temperature patterns in Santa Barbara Channel" by G. S. E. Lagerloef and R. L. Bernstein. *Journal of Geophysical Research*, **91**, 2633–2644.
- Kononen K. and S. Nómmann (1992) Spatio-temporal dynamics of the cyanobacterial blooms in the Gulf of Finland, Baltic Sea. In: *Marine pelagic cyanobacteria: Trichodesmium and other diazotrophs*, E. J. Carpenter *et al.*, editors, Kluwer, Amsterdam, pp. 95–113.
- Kononen K., K. Sivonen and J. Lehtimäki (in press) Toxicity of phytoplankton blooms in the Gulf of Finland and Gulf of Bothnia, Baltic Sea. In: 5th *International Conference on toxic marine phytoplankton*, Rhode Island, October 1991.
- LA VIOLETTE P. E. and R. J. HOLYER (1988) Noise and temperature gradients in multichannel sea surface temperature imagery of the ocean. *Remote Sensing of the Environment*, 25, 231–241.
- McClain E. P., W. G. Pichel and C. C. Walton (1985) Comparative performance of AVHRR-based multichannel sea surface temperatures. *Journal of Geophysical Research*, **90**, 11,587–11,601.
- PAVELSON J. (1988) Nature and characteristics of thermohaline fronts in the Baltic Proper. 16th Conference of the Baltic Oceanographers, Kiel, pp. 796–805.
- Schluessel P., H.-J. Shin, W. J. Emery and H. Grassl (1987) Comparison of satellite-derived sea surface temperatures with *in situ* skin measurements. *Journal of Geophysical Research*, **92**, 2859–2874.
- SIMPSON J. H. and J. R. HUNTER (1974) Fronts in the Irish Sea. Nature, 250, 404-406.
- SIMPSON J. J. (1990) On the accurate detection and enhancement of oceanic features observed in satellite data. Remote Sensing of the Environment, 33, 17–33.
- SIMPSON J. J. and C. Humphrey (1990) An automated cloud screening algorithm for day-time advanced very high resolution radiometer imagery. *Journal of Geophysical Research*, **95**, 13,459–13,481.
- Woods J. (1988) Scale upwelling and primary production. In: *Toward a theory on biological–physical interactions in the world ocean*, B. J. Rotschild, editor, Kluwer, Amsterdam, pp. 7–38.